Scientific paper

Phosphate Ion Removal from Synthetic and Real Wastewater Using $MnFe_2O_4$ Nanoparticles: A Reusable Adsorbent

Widodo Brontowiyono,[1] Indrajit Patra,[2] Shaymaa Abed Hussein,[3] Alimuddin,[4] Ahmed B. Mahdi,[5] Samar Emad Izzat,[6] Dhuha Mohsin Al-Dhalemi,[7,*] Ahmed Kareem Obaid Aldulaim,[8] Rosario Mireya Romero Parra,[9] Luis Andres Barboza Arenas[10] and Yasser Fakri Mustafa[11]

[1] *Department of Environmental Engineering and Centre for Environmental Studies, Islamic University of Indonesia, Yogyakarta-55589, Indonesia*

[2] *An Independent Researcher, Ex Research Scholar at NIT Durgapur, Durgapur, West Bengal, India*

[3] *Al-Manara College for Medical Sciences, Maysan, Iraq*

[4] *Physical Sciences Section, School of Sciences, Maulana Azad National Urdu University, Hyderabad-500032, Telangana, India*

[5] *Anesthesia Techniques Department, Al-Mustaqbal University College, Babylon, Iraq*

[6] *Pharmacy Department, Al-Nisour University College, Baghdad, Iraq*

[7] *Altoosi University College, Najaf, Iraq*

[8] *Department of Pharmacy, Al-Zahrawi University College, Karbala, Iraq*

[9] *Universidad Continental, Lima, Perú*

[10] *Universidad Tecnológica del Perú, Perú*

[11] *Department of Pharmaceutical Chemistry, College of Pharmacy, University of Mosul, Mosul-41001, Iraq*

** Corresponding author: E-mail:_dhuha14@yahoo.com*

Received: 06-29-2022

Abstract

The purpose of this study was to eliminate phosphate (P) from wastewater using $MnFe_2O_4$ nanoparticles. BET, TGA/DTG, FTIR, SEM, TEM, VSM, XRD and EDX/Map analyses were used to determine the $MnFe_2O_4$ surface properties. The specific surface area of the adsorbent was 196.56 m^2/g and VSM analysis showed that the adsorbent has a ferromagnetic property. The maximum P sorption efficiency using $MnFe_2O_4$ (98.52%) was achieved at pH 6, temperature of 55 °C, P concentration of 10 mg/L, time of 60 min, and sorbent dosage of 2.5 g/L, which is a significant value. Also, the thermodynamic study indicated that the P sorption process is spontaneous and endothermic. Moreover, the utmost sorption capacity of P using $MnFe_2O_4$ was 39.48 mg/g. Besides, $MnFe_2O_4$ can be used for up to 6 reuse cycles with high sorption efficiency (>91%). Also, $MnFe_2O_4$ was able to remove phosphate, COD, and BOD_5 from municipal wastewater with considerable removal efficiencies of 82.7%, 75.8%, and 77.3%, respectively.

Keywords: Sorption, $MnFe_2O_4$ nanoparticles, phosphate, wastewater

1. Introduction

Water pollution is a serious problem that can harm any living thing.[1–2] Among different contaminants, phosphate (P) ion pollution is one of the most important environmental issues worldwide. The presence of P at high concentrations in natural water has adverse impacts on water ecology.[3] By increasing the concentration of P in water, algae and other aquatic plants grow and reduce the level of dissolved oxygen and eliminate photosynthesis in water.[4] Detergents and chemical fertilizers are the largest source of P ions. Domestic effluents and running water from fields where phosphate fertilizers are used release large amounts of P ions into natural waters. According to

the EPA, the maximum allowable level and the limit of P ion release in the environment are reported to be 0.1 ppm and less than 0.05 ppm, respectively.[5] Also, the allowable limit of P ions in drinking water is 0.2 ppm and the standard for discharge of phosphate ions into surface water is 6 ppm. The concentration of P in urban, rural, and agricultural wastewaters is very high (between 15–2000 ppm).[5,6] P has a critical role as an essential matter for plant growth in the soil as well as a limiting element in the algae growth and eutrophication phenomenon in water. A concentration of 0.005–0.05 mg/L is required to cause the eutrophication phenomenon.[7] This phenomenon leads to the abundant growth of aquatic plants, the growth of algae, and the imbalance of organisms in water resources. P in surface waters and effluents are commonly found chemically in the form of organic phosphates (such as detergents) and mineral phosphates (polyphosphates and orthophosphates). Organic polyphosphates and phosphates are converted to orthophosphates after hydrolysis and biodegradation.[8]

There are various procedures for wastewater treatment, including reverse osmosis, membrane technology, chemical deposition, ion exchange, nanofiltration, coagulation, and sorption process. Most of the physical processes such as reverse osmosis have high operating costs.[9–11] Among these processes, the sorption process is a suitable method to eliminate P ions, because this process is economical, simple, reversible, low-cost, high selectivity, and high operating speed.[12] P ions are insoluble in water and can be easily sorbed on the sorbent surface. Many adsorbents have been recently utilized for eliminating P ions, including Fe_3O_4,[13] magnetic/clay,[14] chitosan,[15] goethite nanoparticles,[16] aluminum hydroxide modified palygorskite nano-composites,[17] zirconium oxide,[18] sludge derived biochar,[19] and iron/biochar.[20] Magnetic particles have received much attention for elimination of pollutants from sewage due to their simple synthesis, excellent surface area, and considerable removal efficiency of contaminants.[21] MFe_2O_4 (M = Co, Mn, Cu, Zn, Mg) with the structure of cubic spinel or $MO.Fe_2O_3$ shows an important group of iron oxides in which Fe^{3+} and M^{2+} occupy quadrilateral or octahedral sites. MFe_2O_4 magnetic configurations can be engineered by controlling the chemical features of M^{2+} to produce a wide range of magnetic features.[22] Iron-manganese oxide spinel with $MnFe_2O_4$ structure is an example of metal oxides, which has high thermal and mechanical stability. MnF_2O_4 spinel nanocrystalline can be synthesized by various procedures such as microwave, hydrothermal, and chemical co-precipitation processes. One of the main advantages of $MnFe_2O_4$ is its simple synthesis, which distinguishes it from other adsorbents.[21] To control the size of MFe_2O_4 in the chemical coprecipitation method, pH and temperature adjustment is essential.[22] Nanoadsorbents have properties such as high sorption capacity, excellent performance even at low concentration levels and low cost. Also, they are able to be reused in several cycles without major loss in performance.[23] Due to these properties, $MnFe_2O_4$ nanoparticles were used in this research.

The purpose of this work was to eliminate P ions using $MnFe_2O_4$ nanoparticles. $MnFe_2O_4$ was utilized for the first time for removing phosphate. The nanoadsorbent was synthesized by the chemical co-precipitation method and analyzed by various devices like SEM, BET, TEM, FTIR, XRD, TGA-DTG, VSM, and EDX/Map. Also, the impact of various factors was studied on the P ions removal and the best operating conditions were identified. Moreover, kinetic, isotherm, and thermodynamic behaviors of P ion sorption were studied using $MnFe_2O_4$ nanoparticles.

2. Chemicals and Procedures

2. 1. Chemicals and Devices

In this study, several chemicals were utilized to synthesize $MnFe_2O_4$ nanoparticles as well as P ions stock solution, including KH_2PO_4 (purity = 99%, Sandia Co., China), $MnCl_2$ with a purity of 97%, NaOH with a purity of 99%, acetone with a purity of 99%, $(NH_4)_6\ MO_7\ O_{24}$ with a purity of 99%, HCl with a purity of 37%, H_4NO_3V with a purity of 99% (Merck Co., Germany), and $FeCl_3.6H_2O$ (purity = 99%, Sigma Aldrich Co.).

Also, digital scale (FX 300 I model), magnetic stirrer (HPMT 700 model), magnet, oven (DZF-6020 model), pH meter (RPB1000 model) and UV-vis spectrophotometer (Shimadzu 1700 model, Japan) were utilized to weigh materials, heating and mixing, separation of nanoparticles from the solution, drying the sorbent, regulating the sample pH, determining the residual concentration of P ions in the solution, respectively.

2. 2. Preparing Phosphate Stock Solution and $MnFe_2O_4$ Synthesis

KH_2PO_4 salt was employed to prepare the P stock solution. For this purpose, 4.39 g of KH_2PO_4 was added to one liter of distilled water and stirred to dissolve completely in water. Different concentrations of 10, 20, 30, 50, 70, and 100 ppm were prepared by diluting the initial stock solution.

$MnFe_2O_4$ magnetic nanoparticles were synthesized by the chemical co-precipitation approach at 80 °C. For this purpose, 0.1 mol of $MnCl_2$ and 0.2 mol of $FeCl_3.6H_2O$ were dissolved in 100 mL of distilled water and stirred at 80 °C for 20 min by a magnetic stirrer. Next, NaOH (3 molars) was added to the suspension dropwise to regulate the solution pH at 11. The mixture was stirred for 3 h. After that, the solution color changed to black, indicating the synthesis of $MnFe_2O_4$ nanoparticles. The formed nanoparticles were separated from the mixture by a magnet and washed with distilled water and acetone (C_3H_6O) to neutralize (pH = 7). Afterwards, $MnFe_2O_4$ nanoparticles were placed in an oven at 100 °C for 1 day to dry. The

above-mentioned nanoparticles were ground with a mortar and used as a sorbent.[24]

Several analyses were utilized for identifying the features of $MnFe_2O_4$ before and after the process, including BET (JW-DA, China) for measuring the specific surface area, SEM (TESCAN, Czech Republic) for identifying the sorbent morphology, TEM (CM120, The Nederlands) for investigating the particle distribution, EDX/Map (TESCAN, Czech Republic) for specifying the percentage of elements, FTIR (Alpha, BRUKER, Germany) for determining functional groups, XRD (D6792, The Nederlands) for determining the crystalline phases, VSM (7404, LAKE SHORE, USA) for identifying the magnetic strength of the sorbent, and TGA/DTG (PYRIS, PERKIN ELMER, USA) for specifying the thermal stability of the sorbent.

2. 3. Quantitative Determination of P

To produce a suitable reagent for measuring phosphate ions, 12.5 g of $(NH_4)_6\ MO_7\ O_{24}$ was dissolved in 150 mL of distilled water (solution A). In another balloon, 0.625 g of ammonium metavanadate (H_4NO_3V) was dissolved in 150 mL of distilled water and gently heated (solution B). The solution B was added to solution A and stirred for 5 min. Then, 165 mL of HCl was added to the solution A+B and its volume was raised to 500 mL by distilled water. This solution was then used as the reagent. The colorimetric method was used to measure P ions by the reagent. To measure residual P ions after the sorption process, $MnFe_2O_4$ was separated from the solution using a magnet. Then, 10 ml of the solution containing P ions was mixed with 0.5 ml of the reagent solution. Finally, the concentration of P ions was measured by a UV-vis spectrophotometer device (Shimadzu 1700 model, Japan) at a wavelength of 361 nm.

2. 4. Sorption Tests

The P ion sorption tests were performed using $MnFe_2O_4$ nanoparticles as a batch process. The impact of effective factors such as pH (2–11), adsorbent dosage (0.5–4 g/L), time (5–13 min), temperature (25–55 °C), and P ion concentration (10–100 ppm) was studied to remove P ions. For optimization of pH, various solutions were synthesized in different pHs and P ion concentration of 20 mg/L. Then, 2 g/L of MFe_2O_4 was added to the phosphate solutions. Then, the solutions were stirred at 25 °C with a mixing rate of 500 rpm. After 60 min, the remaining concentration of P ion was measured. Also, to investigate the impact of P ion concentration on the sorption efficiency, several experiments were done at various concentrations of P ion (10–100 ppm), pH of 6, the adsorbent dosage of 2.5 g/L, temperature of 55 °C, mixing rate of 500 rpm, and contact time of 60 min. The sorption capacity (q_e) and sorption efficiency (R) were measured using Equations 1 and 2.

$$q_e = \frac{C_i - C_e \times V}{W} \quad (1)$$

$$\mathrm{R}(\%) = \frac{C_i - C_e}{C_i} \times 100 \quad (2)$$

In mentioned equations, C_i, C_e, W, and V are the P initial concentration, the P remaining concentration (ppm), the adsorbent amount (g/L), and the sample volume (L), respectively.[25]

2. 5. Kinetic, Isotherm, and Thermodynamic Behaviors

There are 3 steps in the sorption of contaminants using a sorbent, which can affect the sorption kinetics, including 1) transfer of contaminants from the solution to the adsorbent surface, 2) penetration of contaminants into the pores inside the adsorbent, and 3) sorption of contaminants on the adsorbent inner surface.[26] In this research, pseudo-first order (PFO) and pseudo-second order (PSO) kinetics were employed to investigate P ions sorption. To this end, several experiments were done at different concentrations of P ions (10–100 ppm) and different contact times (5–130 min). Other factors like pH of 6, mixing rate of 500 rpm, the adsorbent dosage of 2.5 g/L, and temperature of 55 °C were considered constant. Equations 3 and 4 describe the PFO and PSO models, respectively:

$$\ln(q_e - q_t) = \ln q_e - K_1\, t \quad (3)$$

$$\frac{t}{q_t} = \frac{1}{K_2 q_e^2} + \frac{t}{q_e} \quad (4)$$

In these models, q_e (mg/g), q_t (mg/g), K_1 (min^{-1}) and K_2 (g/mg.min) are the sorption capacity at equilibrium time, sorption capacity at time t, the PFO kinetic model constant and the PSO kinetic model constant, respectively.[27,28]

Also, sorption isotherms describe the distribution of contaminant molecules on the adsorbent surface. The most important models are the Langmuir, Dubinnin-Radushkevich (D-R) and Freundlich. The Langmuir theory is used for monolayer sorption on a homogeneous surface with an infinite number of identical sites. In this theory, it is assumed that the adsorbent sites are saturated after monolayer sorption. This model is defined below.[29]

$$\frac{C_e}{q_e} = \frac{C_e}{q_{max}} + \frac{1}{K_L q_{max}} \quad (5)$$

In this model, C_e (mg/L), q_{max} (mg/g) and K_L (L/mg) are the P ion equilibrium concentration, the sorption capacity at equilibrium time, and the Langmuir constant, respectively.

Another isotherm model (Freundlich) describes the sorption process on a heterogeneous surface. The follow-

ing relationship defines the Freundlich model:

$$\ln q_e = \ln K_f + \frac{1}{n}\ln C_e \quad (6)$$

Where, K_f (mg/g(L/mg)$^{1/n}$) and n are the Freundlich constants. Also, n indicates whether the sorption process is desirable or not.[30,31]

Moreover, the D-R model is another important isotherm and assumes that the sorption energy on the surface is homogeneous. The D-R linear model is defined below:

$$\ln q_e = \ln q_m - \beta\varepsilon^2 \quad (7)$$

Where, q_m (mol/g), β (mol^2/J^2), and ε are the theory saturation capacity, the mean sorption free energy, and Polanyi potential, respectively. The Polanyi potential is calculated from Equation 8:

$$\varepsilon = R\,T\,Ln\left(1+\frac{1}{C_e}\right) \quad (8)$$

Also, the following relationship describes the type of the sorption process:

$$E = \frac{1}{\sqrt{2\beta}} \quad (9)$$

For E between 8–16 KJ/mol and lower than 8 KJ/mol, the sorption process will be chemical and physical, respectively.[32]

Also, thermodynamic parameters like Gibbs free energy changes (ΔG°), entropy changes (ΔS°), and enthalpy changes (ΔH°) are employed to determine the nature of the sorption process. Using these parameters, it can be determined whether the sorption process is endothermic or exothermic.[27]

$$\Delta G^0 = \Delta H^0 - T\Delta S^0 = -RT\ln K_d \quad (10)$$

$$\ln(K_d) = \frac{\Delta S^0}{R} - \frac{\Delta H^0}{RT} \quad (11)$$

$$K_d = \frac{q_e}{C_e} \quad (12)$$

In these relationships, K_d is the equilibrium constant.

Negative values of ΔG° in various temperatures indicate the spontaneous nature of the sorption process. For –80 kJ/mol < ΔG° < 0 and –400 kJ/mol < ΔG° < –80 kJ/mol, the sorption process will be physical and chemical, respectively.[33] Also, positive values of ΔH° indicate that the sorption process is endothermic and vice versa. Moreover, positive values of ΔS° indicate an increase in the solid-solute surface disorder during the sorption process, and its negative values display a decrease in irregularity in the sorption process.[27] For investigating the thermodynamic behavior of P ion sorption using $MnFe_2O_4$ nanoparticles, several tests were performed in various temperatures (25–55 °C), pH of 6, mixing rate of 500 rpm, nanoparticles dosage of 2 g/L, P ion concentration of 20 mg/L and contact time of 60 min.

2. 6. Desorption Experiments and Reusability of the Adsorbent

To investigate the desorption process, the sorption of P ions was done in optimal conditions using $MnFe_2O_4$ nanoparticles. Next, $MnFe_2O_4$ was separated from the solution and dried. Then, $MnFe_2O_4$ was added to 50 ml of H_2SO_4 solution in various concentrations (1–5 mol/liter) and stirred for 2 h. Next, the adsorbent was separated from the solutions and the concentration of residual P ions was measured. After that, the optimal concentration of H_2SO_4 was obtained to have the highest efficiency. Next, to study the desorption capability and reusability of the adsorbent in eight cycles, H_2SO_4 solution was used at the optimal concentration (4 molar). The desorption percentage of P ions was calculated as follows:

$$Desorption(\%) = \left(\frac{q_1}{q_2}\right)\times 100 \quad (13)$$

Where q_1 and q_2 are the desorption capacity (mg/g) and the sorption capacity (mg/g) of P ions, respectively.[34]

3. Results and Discussion

3. 1. Characteristics of $MnFe_2O_4$

For determining the surface features of $MnFe_2O_4$ nanoparticles such as specific surface area and pore size, BET analysis was used. According to Table 1, the specific surface area, pores volume and average pore size of $MnFe_2O_4$ were 196.56 m^2/g, 0.366 cm^3/g, and 74.49 °A, respectively. The adsorbent pore size shows that $MnFe_2O_4$ is mesoporous. Also, the high specific surface area of the adsorbent shows that contaminants can be adsorbed on the $MnFe_2O_4$ surface. According to previous studies, the specific surface area of $CoFe_2O_4$, $ZnFe_2O_4$,[35] $MgFe_2O_4$,[36] Fe_2O_3 and Fe_3O_4[37] were 71.56, 120.1, 35.2, 150 and 130 m^2/g, respectively, which are lower than our study.

Table 1. Surface features of $MnFe_2O_4$ nanoparticles by BET analysis

BET specific surface area	196.56 m^2/g
Langmuir specific surface area	m^2/g 273.21
Pore volume	cm^3/g 0.366
BJH pore volume	cm^3/g 0.392
Mean pore size	74.49 °A
BJH average width of absorption pores	74.44 °A
BJH average width of desorption pores	67.14 °A

SEM, EDAX, and Mapping analyses were used to determine the morphology of $MnFe_2O_4$ nanoparticles, distribution of elements, active sites on the adsorbent sur-

face, and elemental compositions before and after the P ion sorption process, as shown in Figure 1. SEM image for $MnFe_2O_4$ nanoparticles shows that there are many holes and bumps, which are effective in the phosphate ion sorption (Figure 1 (a)). Also, EDAX and Mapping analyses for $MnFe_2O_4$ nanoparticles indicate several elements such as Fe (46.87%), O (28.5%), and Mn (24.63%) in its surface, which confirm the correct synthesis of $MnFe_2O_4$ nanoparticles (Figure 1 (b and c)). After sorption of P ions, many changes were observed on the $MnFe_2O_4$ surface, which can be due to the sorption of P ions (Figure 1 (d)). Also, EDAX analysis showed that the percentage of elements has been changed. According to Figure 1 (f), the percentages of Fe, O, and Mn were changed to 46.1%, 22.58%, and 30.6%, respectively. Moreover, 0.73% of P was seen after the P ion sorption.

TEM analysis was also employed to determine the morphology and particle size of $MnFe_2O_4$ nanoparticles (Figure 2). The outcomes show that the particle size of $MnFe_2O_4$ is smaller than 50 nm. The particles in the $MnFe_2O_4$ structure have spherical and cubic morphologies with fine size distribution. A similar morphology was observed by Cabrera et al.[38]

Figure 3 indicates FTIR analysis for $MnFe_2O_4$ nanoparticles. For $MnFe_2O_4$ nanoparticles before sorption, a wide peak was seen at 3363 cm^{-1}, which can be attributed to the stretching vibration of hydroxyl group (-OH). Also, another absorption peak was seen at 586 cm^{-1}, which shows the spinel ferrite crystal structure of $MnFe_2O_4$. Also, the absorption peak at 586 cm^{-1} shows intrinsic stretching vibrations of metals at tetrahedral sites.[39] Moreover, two peaks were observed at 1624 cm^{-1} and 964 cm^{-1}, which indicate C = C and C-O vibrations,

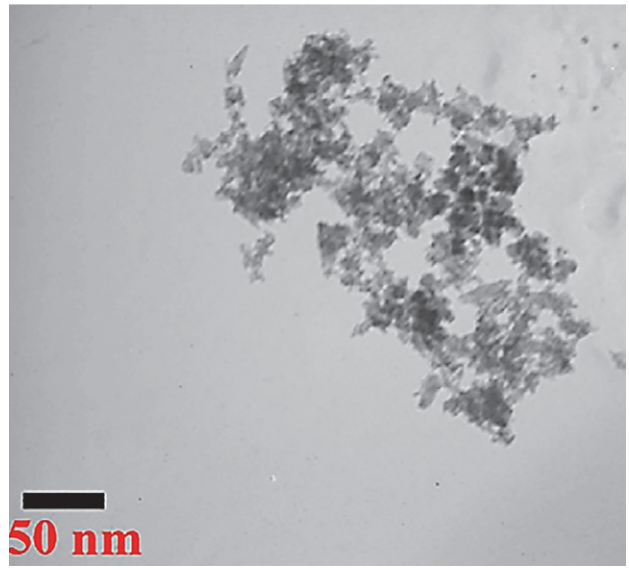

Figure 2. TEM image for $MnFe_2O_4$ nanoparticles

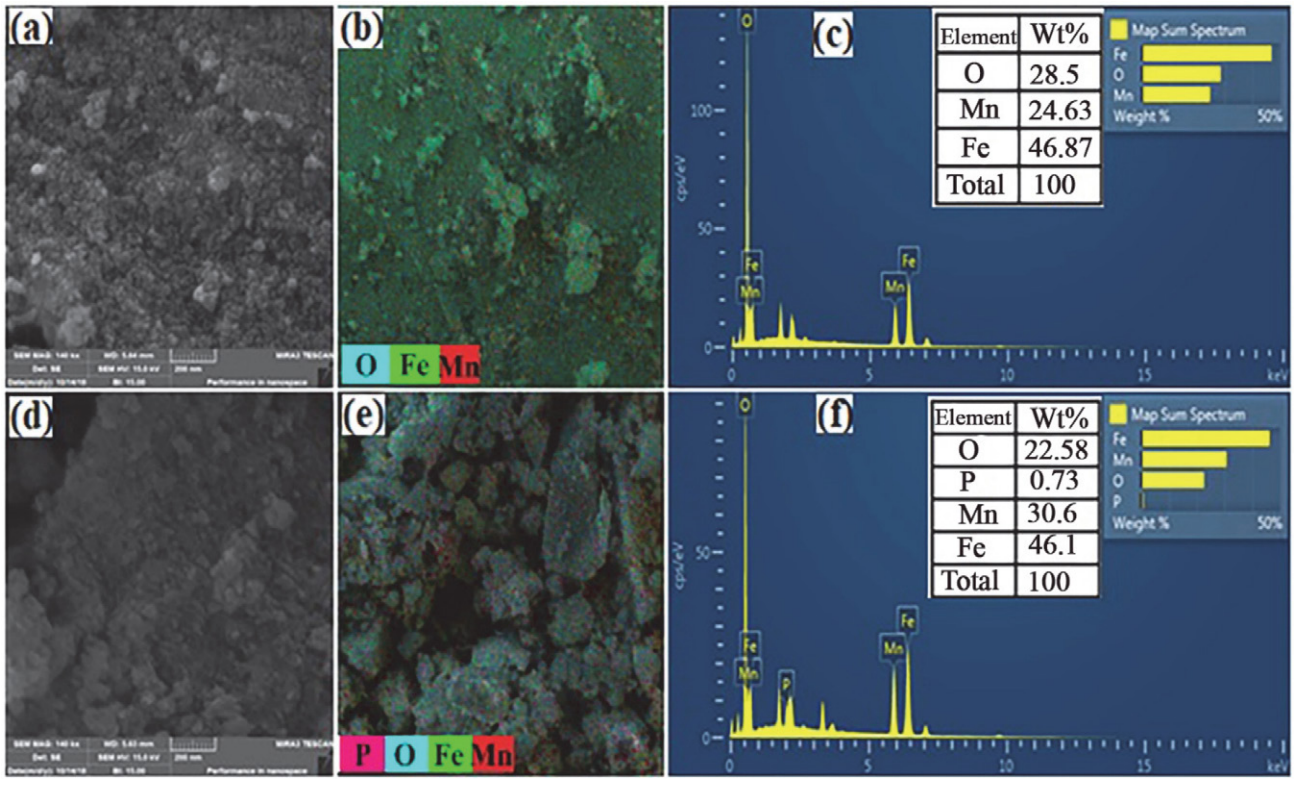

Figure 1. SEM, Mapping, and EDAX analysis for $MnFe_2O_4$ nanoparticles before sorption (a-c) and after sorption of P ions (d-f)

respectively.[24] After sorption of P, the range of absorption peaks in the $MnFe_2O_4$ structure was slightly changed, which can be due to the interaction of functional groups and phosphate ions. To this end, functional groups of -OH, C = C, C-C, and Fe-O in the $MnFe_2O_4$ structure were shifted to 3366, 1632, 1016, and 583 cm^{-1}, respectively.[40–42]

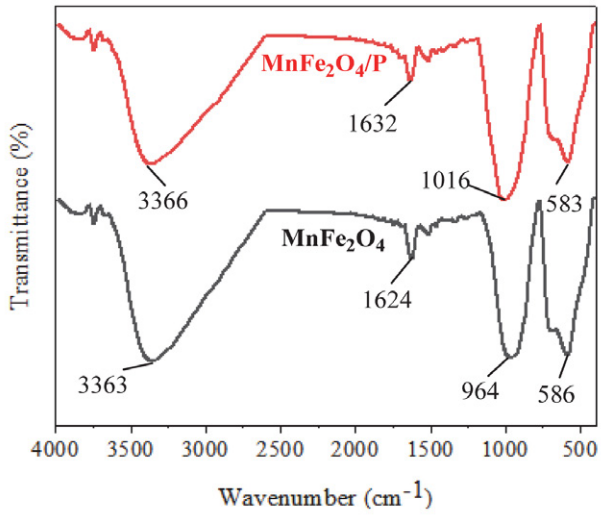

Figure 3. FTIR results for $MnFe_2O_4$ nanoparticles before and after sorption of P ions

Moreover, XRD analysis for determining the crystalline phases in the $MnFe_2O_4$ structure is demonstrated in Figure 4. Several peaks with various intensities were observed at 18.04 °, 29.6 °, and 35.02 °, which are attributed to the crystalline phases of (111), (220), and (311), respectively. Also, other peaks were observed at 42.42 °, 56.62 °, and 61.74 °, which are attributed to the crystalline phases of (400), (422), and (440), respectively. These crystalline phases correspond to the card number 0449-075-01.[24,38] The peak at 35.02° is attributed to the spinel structure of Mn ferrite, which has been confirmed by Cabrera et al.[38]

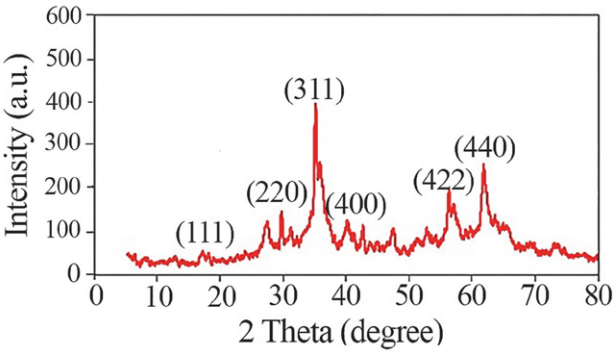

Figure 4. XRD results for $MnFe_2O_4$ nanoparticles

Furthermore, VSM analysis was used to measure the magnetic strength of $MnFe_2O_4$ nanoparticles (Figure 5). According to the results, magnetic saturation, coercive force, and magnetic resonance of $MnFe_2O_4$ nanoparticles were 6.377 emu/g, 230 Oe, and 2.245 emu/g, respectively. The amount of magnetic saturation and the resulting figure shows that $MnFe_2O_4$ nanoparticles have ferromagnetic properties and can be separated from the aqueous media by a magnet (1 Tesla).[43]

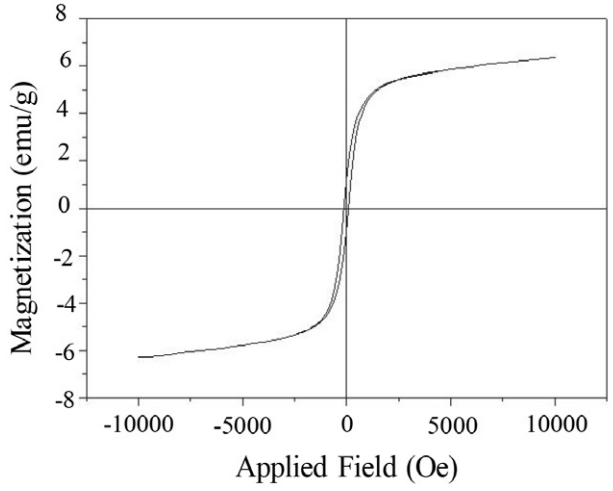

Figure 5. Magnetic behavior of $MnFe_2O_4$ nanoparticles

Eventually, the thermal stability of $MnFe_2O_4$ nanoparticles was investigated by TGA-DTG analysis (Figure 6). In the temperature range of 50–300 °C, $MnFe_2O_4$ nanoparticles lost 5% by weight, which can be due to the evaporation of moisture from its surface.[44] By increasing temperature from 300 to 900 °C, $MnFe_2O_4$ nanoparticles had the highest weight loss (8 wt.%), which is due to the structural degradation and dehydroxylation of $MnFe_2O_4$ nanoparticles.[45] Also, its weight loss in the temperature range of 900–1000 °C was about 2% by weight. Generally, $MnFe_2O_4$ nanoparticles showed a weight loss of 15 wt.%.

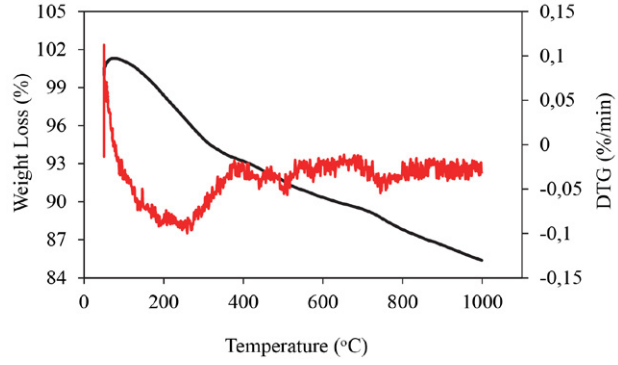

Figure 6. TGA-DTG analysis for thermal stability of $MnFe_2O_4$ nanoparticles

3. 2. Effective Factors on the P Ion Removal

The solution pH is a key factor in the sorption process and can affect the surface properties of the adsorbent. Also, pH causes the release of various forms of ions in the solution.[46] Figure 7 shows the impact of pH at different temperatures on the uptake of P ions. Depending on the solution pH, phosphate species are present in water and seawater as H_3PO_4, H_2PO^{4-}, HPO_4^{2-}, and PO_4^{3-} ions. The pH value of municipal effluent normally is in the range of 6.5–7.3, and $H_2PO_4^-$ species is the major species of phosphate.[47] At pH> 2, H_3PO_4 is the predominant species of P ion in solution, which is due to the absence of electrostatic forces. By increasing the pH from 2 to 6, H_2PO^{4-} and HPO_4^{2-} are the main species in the solution, which have a strong attraction to the $MnFe_2O_4$ adsorbent, enhancing removal efficiency. At pH>6, the sorption efficiency decreases because the solution contains large amounts of $H_2PO_4^-$ and PO_4^{3-} species, and these ions compete fiercely with OH^- ions to sit on the active sites of the adsorbent.[20] Therefore, the highest removal efficiency (96.56%) was obtained at pH 6.

Also, the impact of temperature on the P ion sorption is shown in Figure 7. The tests were performed at the adsorbent dosage of 2 g/L, P ion concentration of 20 mg/L, mixing rate of 500 rpm, time of 60 min, and pH of 6. As shown, the sorption efficiency of P ions enhances from 86.83% to 96.56% with raising the temperature from 25 to 55 °C, respectively, demonstrating that the sorption of P ions using $MnFe_2O_4$ nanoparticles is endothermic.[20] Therefore, the optimal temperature for removing P ions using $MnFe_2O_4$ nanoparticles was 55 °C.

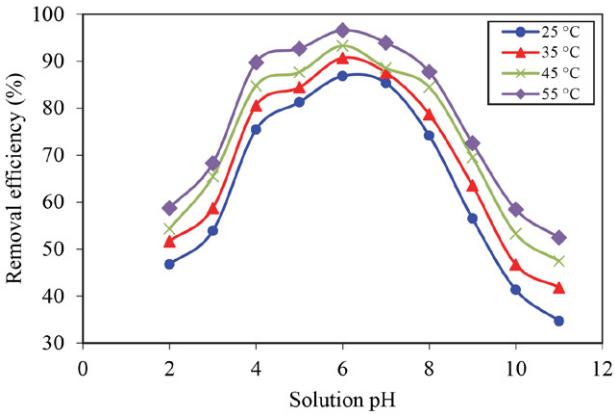

Figure 7. Impact of pH at different temperatures on the P ion sorption using $MnFe_2O_4$ nanoparticles (contact time = 60 min, mixing rate = 500 rpm, pH = 6, P ion concentration = 20 mg/L and adsorbent dosage = 2 g/L)

The initial concentration of P ions in the solution plays an important role as the driving force overcoming the resistance due to the mass transfer between the liquid and solid phases. The impact of phosphate ion concentration at different contact times on the P ion sorption using $MnFe_2O_4$ nanoparticles is indicated in Figure 8. As shown, the removal efficiency of P ions decreases from 97.43% to 87.54% with increasing P ion concentration from 10 to 100 mg/L, respectively, which is due to the greater accessibility of active sites at low P ion concentrations. At a constant adsorbent dose, the ratio of active sites to P ions decreases with increasing P ion concentration, resulting in a decrease in the interaction between P ions and sorption sites.[48,49] Therefore, the highest removal efficiency of P ions (97.43%) was obtained at a concentration of 10 mg/L.

Also, the contact time is a key factor for understanding the equilibrium sorption rate by the adsorbent. The time-dependent sorption provides the sorption rate in which contaminants can be adsorbed on the adsorbent surface.[50] Figure 8 presents the impact of contact time on the P ion sorption efficiency. As shown, the contact time has an impressive impact on the sorption process, so that with increasing time from 5 to 60 min, the P ion sorption efficiency increases from 46.26% to 97.43%, respectively. With increasing contact time, P ions in the solution have a greater chance of being located on $MnFe_2O_4$ sorption sites. However, the removal efficiency decreases at higher contact times, which may be due to the saturation of $MnFe_2O_4$ sorption sites.[51] It can be assumed that the sorption process of P ions using $MnFe_2O_4$ mainly follows intraparticle diffusion and sorption complex mechanisms. Previous researchers have also found the same trend for sorption of other ions.[52] Therefore, 60 min was considered as the optimal contact time.

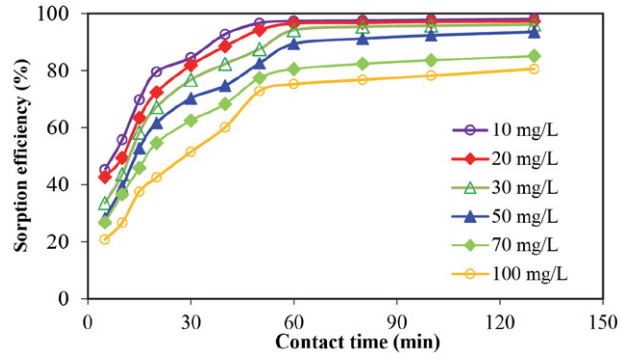

Figure 8. Impact of contact time in various concentrations of P ion on the removal efficiency (Conditions: pH = 6, mixing rate = 500 rpm, adsorbent dosage = 2 g/L, and temperature = 55 °C)

Adsorbent dosage is another critical factor in the P ion sorption efficiency because it directly affects the economics of the process. The removal efficiency and sorption capacity of P ions using $MnFe_2O_4$ nanoparticles in various concentrations of $MnFe_2O_4$ (0.5–4 g/L) are illustrated in Figure 9. It is observed that the P ion removal efficiency increases with increasing $MnFe_2O_4$ concentration from 0.5 to 2.5 g/L, which is due to an increase in sorption sites. At adsorbent dosage> 2.5 g/L, no significant change in removal efficiency was observed because almost all P ions

are adsorbed by the adsorbent and the $MnFe_2O_4$ sorption sites are saturated. Also, the sorption capacity of P ions decreases with increasing $MnFe_2O_4$ concentration. P ions in solution aggregate at high adsorbent dosages, which leads to saturation of the adsorbent surface and thus reduces the sorption capacity.[53–55] According to the results, the utmost sorption capacity of P ions using $MnFe_2O_4$ nanoparticles was attained as 9.172 mg/g. Also, the utmost sorption efficiency (98.52%) was obtained at the adsorbent dosage of 2.5 g/L.

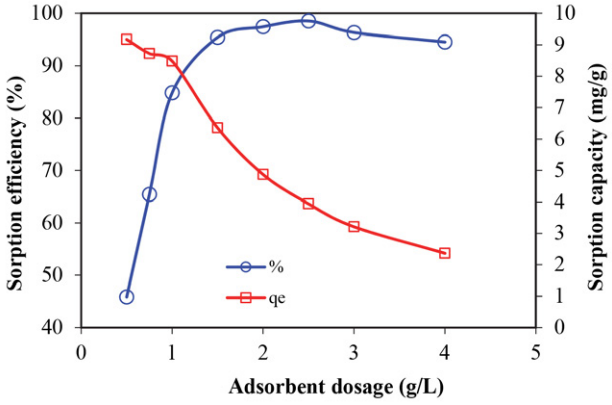

Figure 9. Impact of $MnFe_2O_4$ dose on sorption efficiency and sorption capacity of P ions (Conditions: pH = 6, mixing rate = 500 rpm, P ion concentration = 10 ppm, contact time = 60 min, and temperature = 55 °C)

3. 3. Sorption Isotherms

The Langmuir, D-R, and Freundlich models were used to study the sorption isotherms of P ions using $MnFe_2O_4$ nanoparticles (Figure 10 and Table 2). To this end, several experiments were performed in various P ion concentrations (10–100 ppm). According to the results, the correlation coefficient (R^2) for the Freundlich model (0.978) was higher than the Langmuir (0.973) and D-R (0.814) models, indicating that the Freundlich isotherm model can better describe the P ion sorption process. Also, sorption of P ions occurs in multilayers on the heterogeneous surfaces of $MnFe_2O_4$ nanoparticles. Moreover, the R^2 value for the D-R model was small, indicating that the D-R model is not fitted well with the experimental data. The highest sorption capacity of P ions by the Langmuir model was 39.84 mg/g, which is an acceptable amount. The Langmuir separation factor R_L was also between 0 and 1, indicating that the P ions sorption process is favorable. Besides, the value of n in the Freundlich model was greater than 1, showing that the P ions sorption process using $MnFe_2O_4$ nanoparticles is physical. Using the D-R model, the mean free energy (E) was obtained as 2.331 KJ/mol, which is less than 8 KJ/mol, and shows that the P ion sorption using $MnFe_2O_4$ nanoparticles is physical. The maximum sorption capacity by the D-R model was

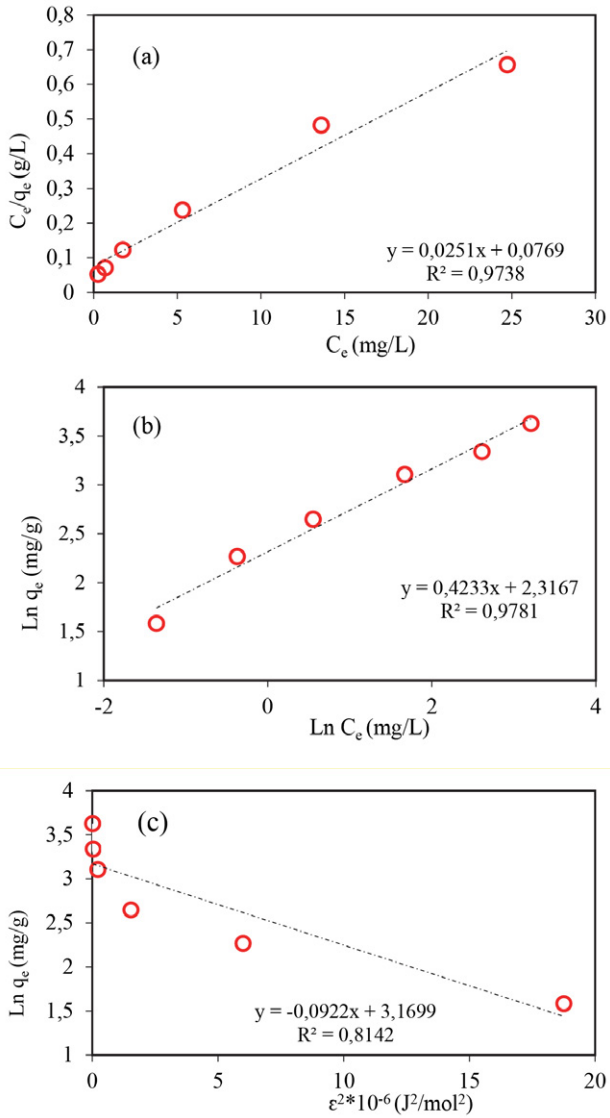

Figure 10. Sorption isotherms of P ions using the Langmuir (a), Freundlich (b) and D-R (c) models (Conditions: pH = 6, $MnFe_2O_4$ dose = 2 g/L, temperature = 55 °C, time = 60 min, mixing rate = 500 rpm)

23.805 mg/g, which is less than the value obtained by the Langmuir model. Also, the Langmuir (K_L) and Freundlich (K_f) model constants were 0.326 L/g and 10.142 mg/g.(L/mg)$^{1/n}$, respectively.

The maximum sorption capacity of P ions using $MnFe_2O_4$ nanoparticles was compared with previous works, as reported in Table 3. As reported, Silica/2-methyl-1-naphthylamine composite with the maximum sorption capacity of 159.12 mg/g[56] and bentonite/magnesium hydroxide with the maximum sorption capacity of 4.3 mg/g[57] showed the highest and lowest sorption capacities. Also, the adsorbent used in this work ($MnFe_2O_4$ nanoparticles) with an utmost sorption capacity of 39.84 mg/g showed a suitable sorption capacity compared to other adsorbents.

Table 2. Parameters of P ions sorption isotherms using $MnFe_2O_4$ nanoparticles

Model	Factor	Value
Langmuir	q_m(mg/g)	39.84
	K_L (L/mg)	0.326
	R^2	0.973
	R_L	0.029–0.234
Freundlich	n	2.362
	K_f (mg/g (L/mg)$^{1/n}$)	10.142
	R^2	0.978
D-R	E (KJ/mol)	2.331
	q_m (mg/g)	23.805
	$\beta \times 10^{+6}$ (mol^2/J^2)	0.092
	R^2	0.814

Table 3. Comparing the maximum sorption capacity of P ions using various adsorbents

Reference	q_{max} (mg/g)	Adsorbent
11	52.1	cross-linked chitosan
12	13	acicular goethite nanoparticles
13	16.86	aluminum hydroxide/ palygorskite nanocomposite
56	159.12	Silica/2-methyl-1-naphthylamine composite
57	4.3	Carboxymethyl cellulose/Fe
58	57.8	Magnetite
58	66.6	Ferrihydrite
58	50.5	Goethite
59	6.722	Chitosan
60	8.21	iron oxide
61	36	Fe-Mn binary oxide
Present study	39.84	$MnFe_2O_4$

3. 4. Sorption Kinetics

Kinetic models determine the sorption mechanisms. They also determine whether the sorption process follows the PFO or PSO kinetic models. The PFO and PSO models were used to study the kinetic behavior of the P ions sorption using $MnFe_2O_4$ nanoparticles. To this end, several experiments were performed at various P ion concentrations from 10 ppm to 100 ppm and different contact times from 5 min to 130 min. The results of sorption kinetics are provided in Figure 11 and Table 4. As reported, the amount of $q_{e,cal}$ in different concentrations of P ions (10, 20, 30, 50, 70, and 100 ppm) for the PFO model were calculated as 3.063, 8.864, 14.042, 20.753, 27.01, and 36.205 mg/g, respectively, while these values for the PSO model were 5.23, 10.548, 16.025, 26.455, 33.67, and 47.46

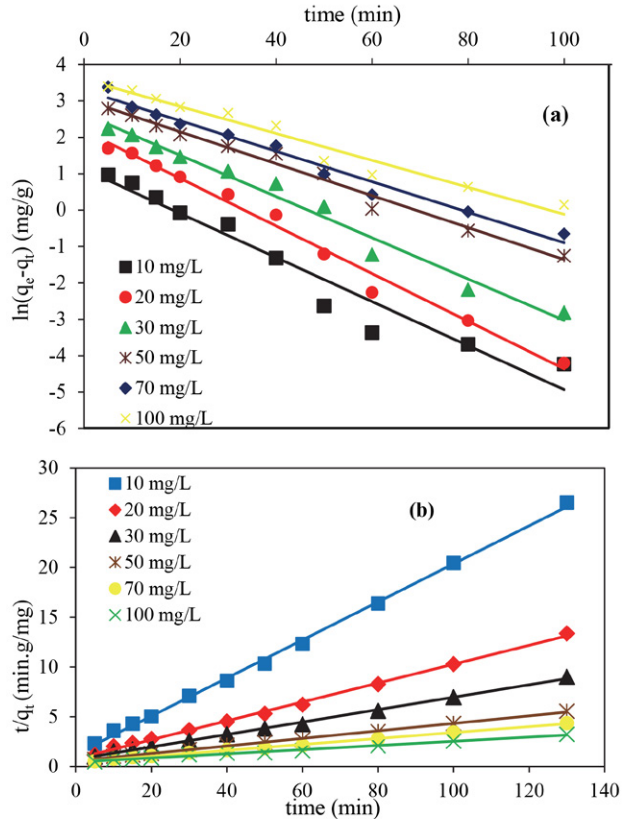

Figure 11. Sorption kinetics of P ions using $MnFe_2O_4$ nanoparticles in different concentrations of P ion (10–100 ppm) and different contact times (5–130 min), including the PFO model (a) and PSO model (b) (Other conditions: adsorbent dosage = 2 g/L, temperature = 55 °C, mixing rate = 500 rpm and pH = 6)

Table 4. Sorption kinetics of P ions using $MnFe_2O_4$ nanoparticles

Kinetic model	Parameter	P ion concentration					
		10 ppm	20 ppm	30 ppm	50 ppm	70 ppm	100 ppm
PFO	R^2	0.9441	0.9887	0.9878	0.985	0.9779	0.9638
	K_1(min^{-1})	0.0605	0.0654	0.0567	0.0439	0.0419	0.037
	$q_{e.cal}$ (mg/g)	3.063	8.864	14.042	20.753	27.01	36.205
	$q_{e.exp}$ (mg/g)	4.906	9.726	14.427	23.38	29.792	40.28
PSO	R^2	0.9985	0.9978	0.9978	0.9979	0.9977	0.992
	K_2 (g/mg.min)	0.029	0.011	0.005	0.002	0.002	0.0009
	$q_{e.cal}$ (mg/g)	5.23	10.548	16.025	26.455	33.67	47.46
	$q_{e.exp}$ (mg/g)	4.906	9.726	14.427	23.38	29.792	40.28

mg/g, respectively, which indicates that the amounts of $q_{e,cal}$ for the PSO model are larger than that of the PFO model at all P ion concentrations. Also, the PFO kinetic constant (K_1) in these concentrations were obtained as 0.0605, 0.0654, 0.0567, 0.0439, 0.0419, and 0.037 min^{-1}, respectively. The kinetic study shows that the PSO model has more ability to describe the kinetic behavior of P ion sorption due to higher R^2 values (R^2>0.99) in different concentrations of P ions compared to the PFO model with R^2 between 0.94–0.98. Moreover, the kinetic constant of the PSO model (K_2) is smaller than K_1 in different concentrations of P ion.[19]

3. 5. Thermodynamic Study of P Ion Sorption

The thermodynamic parameters are calculated through the plot of LnK_d against 1/T, as shown in Figure 12. The thermodynamic constants are also reported in Table 5. As given, negative values of ΔG° in various temperatures (–2.954 kJ/mol at 25 °C and –7.205 kJ/mol at 55 °C) show that the P ion sorption process is spontaneous. Also, the ΔG° values are between 0 to –20 kJ/mol, indicating that the P ion sorption process using $MnFe_2O_4$ nanoparticles is physical. Moreover, ΔH° was a positive value (38.024 kJ/mol), indicating that the P ion sorption process is endothermic, which confirms the results of the impact of temperature on the sorption process. Furthermore, ΔS° was a positive value (136.848 J/mol K), showing that irregularities between the solid (adsorbent) and liquid (solution) phases increase during the P ion sorption process using $MnFe_2O_4$ nanoparticles.[62]

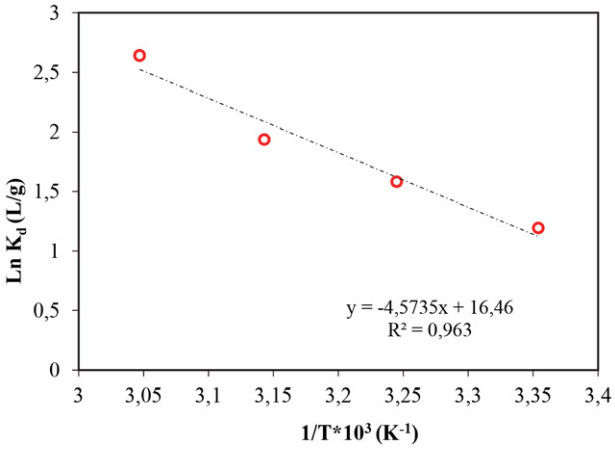

Figure 12. The thermodynamic behavior of P ion sorption using $MnFe_2O_4$ nanoparticles (Conditions: mixing rate = 500 rpm, pH = 6, $MnFe_2O_4$ dose = 2 g/L, P ion concentration = 10 mg/L, and contact time = 60 min)

3. 6. Reusability of $MnFe_2O_4$

The reusability of the adsorbent in different cycles is very important for its industrial applications due to the cost-effectiveness of the process.[63,64] After examining the sorption efficiency of $MnFe_2O_4$ nanoparticles in the removal of P ions from an aqueous solution, the reusability of $MnFe_2O_4$ nanoparticles was studied in eight reuse cycles to assess its industrial utilization potential (Figure 13). The solution containing H_2SO_4 was used to study the reusability of $MnFe_2O_4$. Figure 13 (a) shows the impact of H_2SO_4 concentration on the P ion sorption using $MnFe_2O_4$ nanoparticles. According to the results, the desorption efficiency of P ions increases with increasing H_2SO_4 concentration. However, no significant change was seen in the P ion desorption efficiency at H_2SO_4 concentration above 4 mol/liter. Therefore, the H_2SO_4 concentration of 4 mol/liter was considered the optimum value to study the reusability of $MnFe_2O_4$ nanoparticles. According to Figure 13 (b), $MnFe_2O_4$ nanoparticles were able to remove P ions

Table 5. Thermodynamic parameters for P ion sorption using $MnFe_2O_4$ nanoparticles

Temperature (°C)	ΔG° (kJ/mol)	ΔH° (kJ/mol)	ΔS° (J/mol K)
25	–2.954	38.024	136.848
35	–4.053		
45	–5.123		
55	–7.205		

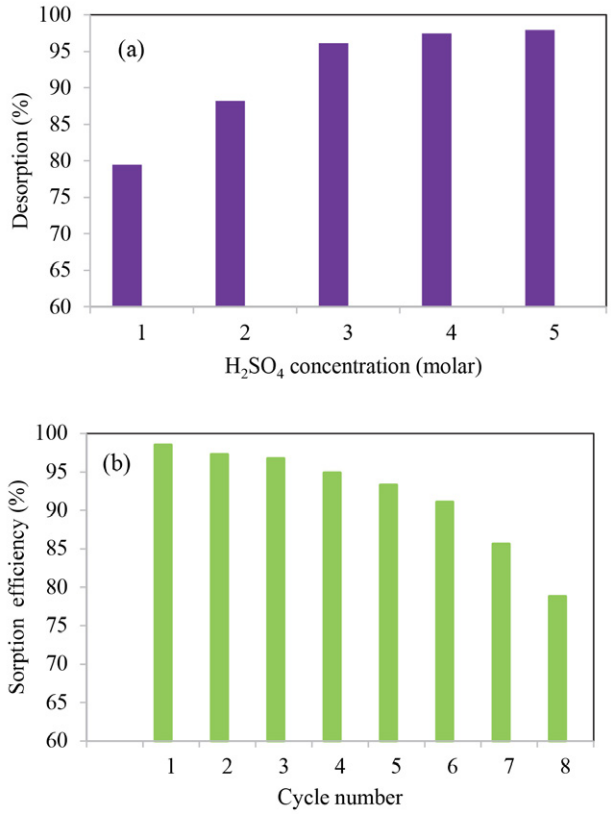

Figure 13. Desorption efficiency (a) and reusability (b) of $MnFe_2O_4$ nanoparticles for removal of P ions from aqueous solution

from an aqueous solution with a sorption efficiency above 91% after six cycles. However, the sorption efficiency of P ions in the 7th and 8th cycles were 85.6 and 78.8%, respectively, which are not suitable sorption efficiencies. Therefore, $MnFe_2O_4$ nanoparticles can be used for up to 6 reuse cycles, which is significant reusability.

3. 7. Treatment of Wastewater Using $MnFe_2O_4$ Nanoparticles

$MnFe_2O_4$ nanoparticles were used to treat urban wastewater and the physical properties of the wastewater before and after treatment are reported in Table 6. As shown, the initial values of COD, BOD_5, pH, and phosphate ions before sorption were 310 ppm, 185 ppm, 9.5, and 22 ppm, respectively. After adding $MnFe_2O_4$ nanoparticles to the wastewater, the values of COD, BOD_5, pH, and phosphate ions were changed to 75 ppm, 42 ppm, 9, and 3.8 ppm, respectively. The results show that the concentration of phosphate ions has been reduced by 82.7%, which is a proper amount. Also, the removal efficiency of COD and BOD_5 using $MnFe_2O_4$ was 75.8% and 77.3%, respectively.

Table 6. The concentration of contaminants in urban wastewater before and after adding $MnFe_2O_4$ nanoparticles

Parameter	Initial value	After treatment	Removal percentage (%)
Phosphate (ppm)	22	3.8	82.7
COD (ppm)	310	75	75.8
BOD_5 (ppm)	185	42	77.3
pH	9.5	9	–

4. Conclusion

The presence of P at high concentrations in water has adverse impacts on water ecology and causes eutrophication. Therefore, the concentration of P in water must be reduced. In this study, the sorption capability of $MnFe_2O_4$ nanoparticles was investigated in the removal of P ions from synthetic and real wastewater. The physical and structural properties of the aforementioned adsorbent were studied by several analyses such as TEM, SEM, EDAX, Mapping, XRD, VSM, FTIR, BET, and TGA. According to these analyses, $MnFe_2O_4$ nanoparticles have a highly porous structure with many active sites, which can be effective in the sorption process. The sorption study indicated that the highest sorption efficiency of P ions was obtained as 98.52%, which was achieved at pH of 6, mixing rate of 500 rpm, $MnFe_2O_4$ dosage of 2.5 g/L, P ion concentration of 10 ppm, temperature of 55 °C and contact time of 60 min. Also, the maximum sorption capacity obtained by the Langmuir model was 39.84 mg/g, which is an acceptable amount compared to other adsorbents for P removal. Moreover, the isotherm and kinetic studies showed that the P ion sorption process using $MnFe_2O_4$ follows the Freundlich and PSO models. Therefore, heterogeneous surfaces of the adsorbent are very important in the P ion sorption process. Furthermore, the D-R and Freundlich isotherm models show that the P ion sorption process using $MnFe_2O_4$ is physical. The thermodynamic factors like ΔG°, ΔS°, and ΔH° displayed that the sorption of P ions using $MnFe_2O_4$ nanoparticles is spontaneous and endothermic. Besides, $MnFe_2O_4$ nanoparticles can be reused for up to 6 cycles with high sorption efficiency. Also, $MnFe_2O_4$ nanoparticles were able to remove COD, BOD_5 and P ions from municipal wastewater with high removal efficiency (>75%). In general, $MnFe_2O_4$ nanoparticles are recommended for industrial wastewater treatment.

Conflict of Interests Statement

No conflict of interests is declared by the authors.

5. References

1. L. Dai, Z. Wang, T. Guo, L. Hu, Y. Chen, C. Chen, G. Yu, L. Q. Ma, J. Chen. *Chemosphere* **2022**, *293*, 133576. **DOI:**10.1016/j.chemosphere.2022.133576
2. W. Liu, J. Zheng, X. Ou, X. Liu, Y. Song, C. Tian, W. Rong, Z. Shi, Z. Dang, Z. Lin. *Environ. Sci. Technol.* **2018**, *52*, 13336–13342. **DOI:**10.1021/acs.est.8b02213
3. Q. Guan, G. Zeng, J. Song, C. Liu, Z. Wang, S. Wu. *J. Environ. Manage.* **2021**, *293*, 112961. **DOI:**10.1016/j.jenvman.2021.112961
4. M. R. Awual, A. Jyo, S. A. El-Safty, M. Tamada, N. Seko. *J. Hazard Mater.* **2011**, *188*, 164–171. **DOI:**10.1016/j.jhazmat.2011.01.092
5. X. Liu, L. Zhang. *Powder Technol.* **2015**, *277*, 112–119. **DOI:**10.1016/j.powtec.2015.02.055
6. M. El Bouraie, A. A. Masoud. *Appl. Clay Sci.* **2017**, *140*, 157–164. **DOI:**10.1016/j.clay.2017.01.021
7. O. Axinte, I. Volf, L. Bulgariu. *Environ. Eng. Manag. J.* **2017**, *16*, 625–631. **DOI:**10.30638/eemj.2017.064
8. C. E. Boyd. Phosphorus. In: *Water Quality. Springer, Cham.* **2015**. **DOI:**10.1007/978-3-319-17446-4_12
9. I. W. Almanassra, V. Kochkodan, G. Mckay, M. A. Atieh, T. Al-Ansari. *J. Environ. Manage.* **2021**, *287*, 112245. **DOI:**10.1016/j.jenvman.2021.112245
10. L. Zhang, L. Wang, Y. Zhang, D. Wang, J. Guo, M. Zhang, Y. Li. *Environ. Res.* **2022**, *206*, 112629. **DOI:**10.1016/j.envres.2021.112629
11. W. Liu, J. Li, J. Zheng, Y. Song, Z. Shi, Z. Lin, L. Chai. *Environ. Sci. Technol.* **2020**, *54*, 11971–11979. **DOI:**10.1021/acs.est.0c01855
12. I. S. Bădescu, D. Bulgariu, I. Ahmad, L. Bulgariu. *J. Environ. Manage.* **2018**, *224*, 288–297. **DOI:**10.1016/j.jenvman.2018.07.066
13. S. Y. Yoon, C. G. Lee, J. J. H. Park, S. B. Kim, S. H. Lee, J. W.

Choi. *Chem. Eng. J.* **2014**, *236*, 341–347. **DOI:**10.1016/j.cej.2013.09.053
14. J. Chen, L. G. Yan, H. Q. Yu, S. Li, L. L. Qin, G. Q. Liu, Y. F. Li, B. Du. *Chem. Eng. J.* **2016**, *287*, 162–172. **DOI:**10.1016/j.cej.2015.11.028
15. M. H. Mahaninia, L. D. Wilson. *J. Colloid Interface Sci.* **2017**, *485*, 201–212. **DOI:**10.1016/j.jcis.2016.09.031
16. R. F. Moreira, S. Vandresen, D. B. Luiz, H. J. José, G. L. Puma. *J. Environ. Chem. Eng.* **2017**, *5*, 652–659. **DOI:**10.1016/j.jece.2016.12.018
17. M. Pan, X. Lin, J. Xie, X. Huang. *RSC Adv.* **2017**, *7*, 4492–4500. **DOI:**10.1039/C6RA26802A
18. K. Qin, F. Li, S. Xu, T. Wang, C. Liu. *Chem. Eng. J.* **2017**, *322*, 275–280. **DOI:**10.1016/j.cej.2017.04.046
19. S. Saadat, E. Raei, N. Talebbeydokhti. *J. Environ. Manage.* **2018**, *225*, 75–83. **DOI:**10.1016/j.jenvman.2018.07.037
20. Q. Yang, X. Wang, W. Luo, J. Sun, Q. Xu, F. Chen, J. Zhao, S. Wang, F. Yao, D. Wang, X. Li. *Bioresour. Technol.* **2018**, *247*, 537–544. **DOI:**10.1016/j.biortech.2017.09.136
21. T. Shanmugavel, S. G. Raj, G. R. Kumar, G. Rajarajan. *Phys. Procedia* **2014**, *54*, 159–163. **DOI:**10.1016/j.phpro.2014.10.053
22. S. Sun, H. Zeng, D. B. Robinson, S. Raoux, P. M. Rice, S. X. Wang, G. Li. *J. Am. Chem. Soc.* **2004**, *126*, 273–279. **DOI:**10.1021/ja0380852
23. M. R. Awual, A. M. Asiri, M. M. Rahman, N. H. Alharthi. *Chem. Eng. J.* **2019**, *363*, 64–72. **DOI:**10.1016/j.cej.2019.01.125
24. M. Ghobadi, M. Gharabaghi, H. Abdollahi, Z. Boroumand, M. Moradian. *J. Hazard. Mater.* **2018**, *351*, 308–316. **DOI:**10.1016/j.jhazmat.2018.03.011
25. M. R. Awual, T. Yaita, S. Suzuki, H. Shiwaku. *J. Hazard. Mater*. **2015**, *291*, 111–119. **DOI:**10.1016/j.jhazmat.2015.02.066
26. M. H. Dehghani, D. Sanaei, I. Ali, A. Bhatnagar. *J. Mol. Liq.* **2016**, *215*, 671–679. **DOI:**10.1016/j.molliq.2015.12.057
27. İ. Şentürk, M. Alzein. *Acta Chim. Slov*. **2020**, *67*, 55–69. **DOI:**10.17344/acsi.2019.5195
28. D. Ge, H. Yuan, J. Xiao, N. Zhu, *Sci. Total Environ*. **2019**, *679*, 298–306. **DOI:**10.1016/j.scitotenv.2019.05.060
29. M. R. Awual, M. M. Hasan, A. Islam, M. M. Rahman, A. M. Asiri, M. A. Khaleque, M. C. Sheikh. *J. Clean. Prod*. **2019**, *228*, 778–785. **DOI:**10.1016/j.jclepro.2019.04.280
30. A. Syafiuddin, S. Salmiati, J. Jonbi, M. A. Fulazzaky. *J. Environ. Manage.* **2018**, *218*, 59–70. **DOI:**10.1016/j.jenvman.2018.03.066
31. B. Bai, D. Rao, T. Chang, Z. Guo. *J. Hydrol*. **2019**, *578*, 124080. **DOI:**10.1016/j.jhydrol.2019.124080
32. J. Mittal, A. Mariyam, F. Sakina, R. T. Baker, A. K. Sharma, A. Mittal. *J. Clean. Prod*. **2021**, *321*, 129060. **DOI:**10.1016/j.jclepro.2021.129060
33. R. A. Rashid, A. H. Jawad, M. A. M. Ishak, N. N. Kasim. *Desalin. Water Treat*. **2016**, *57*, 27226–27236. **DOI:**10.1080/19443994.2016.1167630
34. N. El Messaoudi, M. El Khomri, Z. Goodarzvand Chegini, N. Chlif, A. Dbik, S. Bentahar, M. Iqbal, A. Jada, A. Lacherai. *Int. J. Environ. Anal. Chem*. **2021**. **DOI:**10.1080/03067319.2021.1912338
35. R. Ramadan, N. Shehata. *DESALIN. WATER TREAT*. **2021**, *227*, 370–383. **DOI:**10.5004/dwt.2021.27248
36. A. Doi, M. Nishibori, K. Obata, T. Suzuki, K. Shimanoe, S. Matsushima. *J. Ceram. Soc. JAPAN* **2016**, *124*, 777–780. **DOI:**10.2109/jcersj2.16042
37. S. Lavrynenko, A. G. Mamalis, D. Sofronov, A. Odnovolova, V. Starikov. *Mater Sci Forum* **2018**, *915*, 116–120. **DOI:**10.4028/www.scientific.net/MSF.915.116
38. L. I. Cabrera, Á. Somoza, J. F. Marco, C. J. Serna, M. Puerto Morales. *J. Nanopart. Res*. **2012**, *14*, 1–14. **DOI:**10.1007/s11051-012-0873-x
39. R. S. Yadav, I. Kuřitka, J. Vilcakova, T. Jamatia, M. Machovsky, D. Skoda, P. Urbánek, M. Masař, M. Urbánek, L. Kalina, J. Havlica. *Ultrason. Sonochem*. **2020**, *61*, 104839. **DOI:**10.1016/j.ultsonch.2019.104839
40. R. Liu, L. Chi, X. Wang, Y. Wang, Y. Sui, T. Xie, H. Arandiyan. *Chem. Eng. J.* **2019**, *357*, 159–168. **DOI:**10.1016/j.cej.2018.09.122
41. L. Zhang, Y. Xu, H. Liu, Y. Li, S. You, J. Zhao, J. Zhang. *J. Water Process Eng*. **2021**, *44*, 102368. **DOI:**10.1016/j.jwpe.2021.102368
42. Y. Zhang, Z. Pan, J. Yang, J. Chen, K. Chen, K. Yan, X. Meng, X. Zhang, M. He. *Powder Technol*. **2022**, *399*, 117193. **DOI:**10.1016/j.powtec.2022.117193
43. K. Mensah, H. Mahmoud, M. Fujii, H. Shokry. *J. Water Process Eng.* **2022**, *45*, 102512. **DOI:**10.1016/j.jwpe.2021.102512
44. C. Cannas, A. Falqui, A. N. N. A. Musinu, D. Peddis, G. Piccaluga. *J. Nanopart. Res.* **2006**, *8*, 255–267. **DOI:**10.1007/s11051-005-9028-7
45. M. Artus, S. Ammar, L. Sicard, J. Y. Piquemal, F. Herbst, M. J. Vaulay, F. Fiévet, V. Richard, *Chem. Mater.* **2008**, *20*, 4861–4872. **DOI:**10.1021/cm702464e
46. D. Gugała-Fekner. *Acta Chim. Slov*. 2018, 65, 119–126. **DOI:**10.17344/acsi.2017.3652
47. M. R. Awual, M. A. Shenashen, A. Jyo, H. Shiwaku, T. Yaita. *J. Ind. Eng. Chem*. **2014**, *20*, 2840–2847. **DOI:**10.1016/j.jiec.2013.11.016
48. C. Shi, Z. Wu, F. Yang, Y. Tang. *Solid State Sci.* **2021**, *119*, 106702. **DOI:**10.1016/j.solidstatesciences.2021.106702
49. H. Liu, T. Chen, X. Zou, Q. Xie, C. Qing, D. Chen, R. L. Frost. *Chem. Eng. J.* **2013**, *234*, 80–87. **DOI:**10.1016/j.cej.2013.08.061
50. M. R. Awual, M. M. Hasan, A. M. Asiri, M. M. Rahman. *Compos. B Eng.* **2019**, *171*, 294–301. **DOI:**10.1016/j.compositesb.2019.05.078
51. D. Xu, J. Liu, T. Ma, X. Zhao, H. Ma, J. Li. Environ. Technol. Innov. **2022**, *26*, 102264. **DOI:**10.1016/j.eti.2021.102264
52. R. M. Kamel, A. Shahat, W. H. Hegazy, E. M. Khodier, M. R. Awual. *J. Mol. Liq*. **2019**, *285*, 20–26. **DOI:**10.1016/j.molliq.2019.04.060
53. U. Fegade, G. Jethave, K. Y. Su, W. R. Huang, R. J. Wu. *J. Environ. Chem. Eng.* **2018**, *6*, 1918–1925. **DOI:**10.1016/j.jece.2018.02.040
54. L. R. Bonetto, F. Ferrarini, C. De Marco, J. S. Crespo, R. Guégan, M. Giovanela. *J. Water Process Eng.* **2015**, *6*, 11–20. **DOI:**10.1016/j.jwpe.2015.02.006

55. W. Liu, F. Huang, Y. Liao, J. Zhang, G. Ren, Z. Zhuang, J. Zhen, Z. Lin, C. Wang. *Angew. Chem.* **2008**, *120*, 5701–5704. **DOI:**10.1002/ange.200800172
56. M. R. Awual. *J. Clean. Prod*. 2019, 228, 1311–1319. **DOI:**10.1016/j.jclepro.2019.04.325
57. L. T. Eberhardt, S. H. Min, J. S. Han. *Bioresour. Technol*. **2006**, *97*, 2371–2376. **DOI:**10.1016/j.biortech.2005.10.040
58. Z. Ajmal, A. Muhmood, M. Usman, S. Kizito, J. Lu, R. Dong, S. Wu. *J. Colloid Interface Sci.* **2018**, *528*, 145–155. **DOI:**10.1016/j.jcis.2018.05.084
59. X. Cui, H. Li, Z. Yao, Y. Shen, Z. He, X. Yang, H. Y. Ng, C. H. Wang. *J. Clean. Prod.* **2019***, 207*, 846–856. **DOI:**10.1016/j.jclepro.2018.10.027
60. L. Zeng, X. Li, J. Li. *Water Res.* **2004**, *38*, 1318–1326. **DOI:**10.1016/j.watres.2003.12.009
61. G. Zhang, H. Liu, R. Liu, J. Qu. *J. Colloid Interface Sci.* **2009**, *335*, 168–174. **DOI:**10.1016/j.jcis.2009.03.019
62. X. Lin, K. Lu, A. K. Hardison, Z. Liu, X. Xu, D. Gao, J. Gong, W. S. Gardner. *Ecol. Indic*. **2021**, *126*, 107639. **DOI:**10.1016/j.ecolind.2021.107639
63. M. R. Awual, A. Jyo. *Desalination* **2011**, *281*, 111–117. **DOI:**10.1016/j.desal.2011.07.047
64. X. Tian, R. Yang, T. Chen, Y. Cao, H. Deng, M. Zhang, X. Jiang. *J. Hazard. Mater*. **2022**, *426*, 128121. **DOI:**10.1016/j.jhazmat.2021.128121

Povzetek

Namen te raziskave je odstraniti fosfat (P) iz odpadne vode z uporabo nanodelcev $MnFe_2O_4$. Za določitev površinskih lastnosti $MnFe_2O_4$ so bile uporabljene analize BET, TGA/DTG, FTIR, SEM, TEM, VSM, XRD in EDX/Map. Specifična površina adsorbenta je bila 196,56 m^2/g, analiza VSM pa je pokazala, da ima adsorbent feromagnetne lastnosti. Največja učinkovitost sorpcije P z uporabo $MnFe_2O_4$ (98,52 %) je bila dosežena pri pH 6, temperaturi 55 °C, koncentraciji P 10 mg/L, času 60 min in odmerku sorbenta 2,5 g/L, kar je pomembna vrednost. Poleg tega je termodinamična študija pokazala, da je proces sorpcije P spontan in endotermičen. Največja sorpcijska kapaciteta P z uporabo $MnFe_2O_4$ je bila 39,48 mg/g. $MnFe_2O_4$ se lahko uporablja za do 6 ciklov ponovne uporabe z visoko sorpcijsko učinkovitostjo (>91 %). Poleg tega je $MnFe_2O_4$ odstranil fosfat, KPK in BPK5 iz komunalne odpadne vode s precejšnjo učinkovitostjo odstranjevanja, in sicer 82,7 %, 75,8 % in 77,3 %.